A Search for $B^+ \to K^+ \nu \overline{\nu}$ with *BABAR*

by

Paul D. Jackson

Abstract

The study of flavor-changing neutral current decays is of fundamental interest. They provide a sensitive window in which to search for possible new physics effects beyond the Standard Model of particle physics. Measurements of these processes at rates significantly above the Standard Model would point, unambiguously, to new physics. One such decay of interest is $B^+ \to K^+ \nu \overline{\nu}$. Herein, we discuss the search for this decay mode using 56 million $B\overline{B}$ decays, a dataset approximately 5 times greater than has previously been used to search for this mode. This search exploits a new technique in which a $B^- \to D^0 \ell^- \overline{\nu} X$ decay, which provides both high efficiency and good purity, is used to reconstruct the companion B in the event leaving the remainder to search for a signal consistent with coming from a $B^+ \to K^+ \nu \overline{\nu}$ decay.

Table 1: The three fermion families.

	First Generation	Second Generation	Third Generation	Electric Charge
Quarks	u	c	t	$+2/3$
	d	s	b	$-1/3$
Leptons	e	μ	τ	-1
	ν_e	ν_μ	ν_τ	0

1 Introduction

1.1 The Standard Model

The Standard Model(SM) of particle physics describes the interactions between leptons, quarks and gauge bosons. For each lepton and quark there exists a corresponding anti-particle with the same mass. The quantum numbers given to anti-particles are negative to those of particles. Leptons and quarks have a half-integer spin (collectively known as fermions) and can be classified into three categories referred to as generations or families (see table 1). Within each of these generations, the leptons and quarks are arranged in doublets. These doublets are based on the preference of the charged weak force to couple members of the same doublet. The quark doublets observed in nature are actually a linear combination of the mass states given in table 1.

There are four, known fundamental forces of nature: gravitational, weak, electromagnetic and strong forces. In quantum field theory interactions between particles are described in terms of the exchange of field particles with integer spin, called gauge bosons. The respective mediators of each force are listed in table 2. Neutrinos (ν) are neutral particles that interact only weakly with matter. Charged leptons however, participate in the weak and electromagnetic forces. Quarks, in addition to both the electromagnetic and weak forces, also interact via the strong force. Composite particles made up of quarks are called hadrons and isolated quarks are not found due to the nature of the strong force as its strength increases with distance. When one attempts to separate bound quarks the potential energy involved becomes so large that a new quark-antiquark pair is produced. These then combine to form a new hadron in a process called hadronization. Stable hadrons can be formed in two ways, using 3 quarks/anti-quarks (combinations known as baryons) or in a $q\overline{q}$ pair (called mesons).

The Cabibbo-Kobayashi-Maskawa (CKM) matrix, V_{CKM}, describes the relative size of the charged-current weak amplitudes between quarks. For the reaction $q \rightarrow W^{*-}Q$, where q is a $-1/3$ charged quark and Q has a charge of $+2/3$, the coupling is $g\,V_{Qq}$, where V_{Qq} can in general be complex and g is a universal coupling constant, which is commonly written in terms of $\sin^2\theta_W$ (where θ_W is the Weinberg weak mixing angle) and the electromagnetic charge.

For the reaction $Q \rightarrow W^{*+}q$, the coupling is $g\,V_{Qq}^*$. With three generations, V_{CKM} is a 3 x 3 matrix :

Table 2: The mediators of the four fundamental forces of nature. Note that the graviton has yet to be observed experimentally.

Force	Boson
Gravitational	graviton
Electromagnetic	photon (γ)
Weak	$W^{\pm}$, Z^0
Strong	gluon (g)

$$V_{\text{CKM}} = \begin{pmatrix} V_{ud} & V_{us} & V_{ub} \\ V_{cd} & V_{cs} & V_{cb} \\ V_{td} & V_{ts} & V_{tb} \end{pmatrix}. \tag{1}$$

V_{CKM} provides a connection between quark mass eigenstates ($q = (d,\ s,\ b)$) and weak current eigenstates ($q' = (d',\ s',\ b')$), so that $q' = V_{\text{CKM}}q$. In this way, V_{CKM} as written here is unitary, assuming that there exists exactly three generations of quarks. Additional generations would be denoted as extra columns and rows in the matrix.

Due to the mass of the bottom quark being much lower than that of the top quark, the B meson[1] sector can provide an experimentally accessible way to directly probe the third generation. A collider with a center-of-mass energy equal to that of the $\Upsilon(4S)$ resonance is the ideal place to study the B meson decay, as this resonance decays almost entirely to $B\overline{B}$ pairs. Moreover, an asymmetric machine is even more favorable since this will improve the separation of the two B decay vertices in the laboratory frame allowing time-dependent properties of the mesons to be studied. These properties are exploited by the PEP-II and KEK colliders at which the *BABAR* [1] and BELLE [2] experiments are situated. These detectors are designed for the study of CP violation in the B sector. High luminosity machines are preferred in order to obtain sufficiently high statistics and make rare reactions experimentally feasible to study.

The search for rare B decays can provide a sensitive window in which to search for new physics (NP). They offer a complimentary strategy through searches for the indirect effects of higher order processes. Flavor-changing neutral current (FCNC) decays are one example of such processes. Probing loop-induced couplings at the level of radiative corrections where the top quark plays a major role can provide a sensitive handle on the matrix elements V_{ts} and V_{td} from V_{CKM} in equation 1. Observations of radiative B decays, such as $b \to s\gamma$ at CLEO [3, 4], see figure 2, have provided bounds on CKM ratios such as $|V_{ts}/V_{cb}|$ as well as powerful constraints on NP. Most classes of models which induce large effects in FCNC decays also affect $B_d^0 - \overline{B}_d^0$ mixing. These decays provide useful insight into higher-order couplings and if large deviations from SM expectations are observed there are models which may point to NP.

---

[1]A B meson is composed of a $\overline{b}$ quark combined with either a u, in the charged B case, or d in the case of a neutral B. Charged conjugate modes are implied.

1.2 Theoretical background to the analysis

The investigation of FCNC decays is of fundamental interest. In SM these decays are forbidden at tree level, and occur only in loop diagrams. As a result, their rates are highly suppressed. The SM prediction for the FCNC decay $b \to s\nu\overline{\nu}$ is nearly free from strong interaction effects and has very small theoretical uncertainty. An observation of this decay at a level significantly above the SM prediction would provide unambiguous evidence for new physics. Within the SM the decay
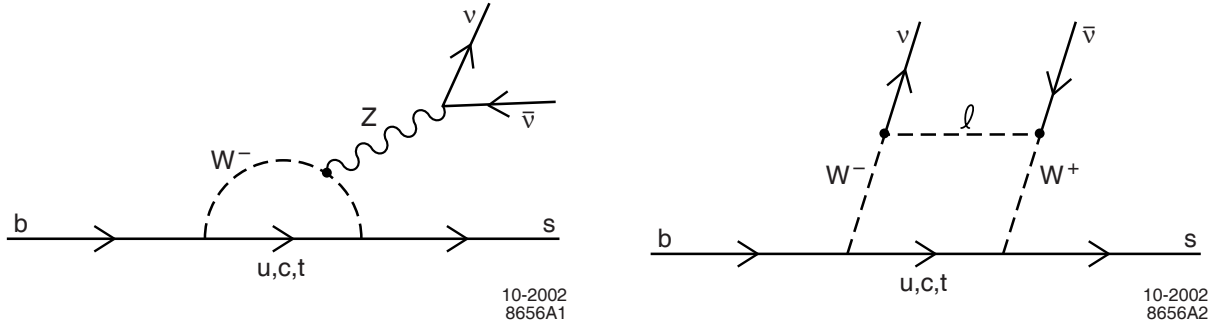

Figure 1: Standard Model Feynman diagrams for $B \to X_s \nu\overline{\nu}$

$b \to s\nu\overline{\nu}$ proceeds through W box diagrams and Z penguin diagrams, figure 1 shows the Feynman diagrams for these processes. The expected branching fraction, summed over all neutrino species, is [5]

$$\mathcal{B}(b \to s\nu\overline{\nu}) = \left(4.1^{+0.8}_{-1.0}\right) \times 10^{-5} \quad . \tag{2}$$

At present it does not appear to be feasible to search for the inclusive decay $b \to s\nu\overline{\nu}$; however, the decay $B^+ \to K^+\nu\overline{\nu}$ is tractable. The expected branching fraction for $B^+ \to K^+\nu\overline{\nu}$, summed over all neutrino species, is [6]

$$\mathcal{B}(B^+ \to K^+\nu\overline{\nu}) = \left(0.38^{+0.12}_{-0.06}\right) \times 10^{-5} \quad . \tag{3}$$

The best previous experimental limit is $\mathcal{B}(B^+ \to K^+\nu\overline{\nu}) < 2.4 \times 10^{-4}$ at 90% confidence level [7].

In order to study the $b \to s$ transition and the couplings involved we can write down an effective Hamiltonian describing the more general $b \to q\nu_f\overline{\nu}_f$ transition, where $q = d, s$ and $f = e, \mu, \tau$. Within the SM this is given by,[2]

$$H_{\text{eff}}^f = \frac{4G_F}{\sqrt{2}} \frac{\alpha}{2\pi \sin^2 \theta_W} \sum_{i=u,c,t} V_{ib} V_{iq}^* c_L^i(m_i)(\overline{q}\gamma_\mu P_L b)(\overline{\nu}_f \gamma^\mu P_L \nu_f) \tag{4}$$

where,

$$P_{L,R} = \frac{(1 \mp \gamma_5)}{2} \tag{5}$$

---

[2]We suppress the neutrino flavor index, f, carried by the Wilson coefficients throughout what is to follow.

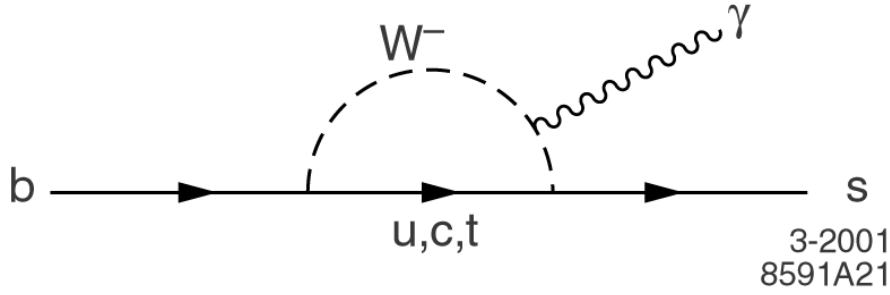Figure 2: Standard Model Feynman diagram for $b \to s\gamma$

and $\tilde{c}_L^i(m_i)$ represents the contributions from the internal quarks $i = u, c, t$, and m_i are their corresponding masses. This can be further simplified to,

$$H_{\text{eff}}^f = \frac{4G_F}{\sqrt{2}} \frac{\alpha}{2\pi \sin^2 \theta_W} \sum_{i=c,t} V_{ib} V_{iq}^* c_L^i(m_i)(\overline{q}\gamma_\mu P_L b)(\overline{\nu}_f \gamma^\mu P_L \nu_f), \qquad (6)$$

with $c_L^i(0) = 0$. [Note that in equation 6 we take the limit $m_u \to 0$.]

Exploiting the fact that

$$\frac{c_L^c(m_c)}{c_L^t(m_t)} \sim O(10^{-3}), \quad \left| \frac{V_{cb} V_{cq}^*}{V_{tb} V_{tq}^*} \right| \sim O(1) \ \ (q = d, s), \qquad (7)$$

the charm-quark contribution to the quark-level process $b \to q\nu_f \overline{\nu}_f$ can be safely neglected, and we arrive at

$$H_{\text{eff}}^f = \frac{4G_F}{\sqrt{2}} \frac{\alpha}{2\pi \sin^2 \theta_W} V_{tb} V_{tq}^* c_L^t(m_t)(\overline{q}\gamma_\mu P_L b)(\overline{\nu}_f \gamma^\mu P_L \nu_f). \qquad (8)$$

Equation 8 includes the couplings V_{tb} and V_{tq}^* and since this equation has a relatively simple form it exhibits the theoretical cleanliness of the $b \to q\nu_f \overline{\nu}_f$ transition.

1.3 Enhancement from contributions beyond SM

With the possibility of exotic new effects manifesting themselves within the loops of the diagrams shown in figure 1 it is no surprise that theorists have developed a multitude of ideas to explain any possible increase to the SM rate of $b \to s\nu\overline{\nu}$. Many of these theories also affect the decays $b \to s\gamma$ [3,4] and $b \to s\ell^+\ell^-$ [10–12] in a similar way. As these decays have already been measured their values put constraints on the possible models which can effect the $b \to s\nu\overline{\nu}$ reaction[3].

The radiative $B \to X_s\gamma$ decay proceeds via photonic penguin diagrams, and therefore it is not directly related to $B \to X_s\nu\overline{\nu}$. However, in many models the details of the underlying physics imply relations between the Z and photonic penguins. In all such models the CLEO measurement

---

[3]The context of beyond the SM physics will be discussed in terms of the $B \to X_s\nu\overline{\nu}$ reaction and not the exclusive $B^+ \to K^+\nu\overline{\nu}$ decay as most effects will manifest themselves in all such exclusive modes.

of $B \to X_s\gamma$ [3, 4], which is in agreement with the SM, forbids large deviations from the SM predictions for the $B \to X_s\nu\overline{\nu}$ decay rate as well.

On the other hand a large class of NP models predict (or can at least accomodate) an enhanced bsZ effective vertex without giving rise to a large enhancement of the $bs\gamma$ effective coupling. Then constraints from inclusive and exclusive $B \to X_s\ell^+\ell^-$ decays are important, as these decays, like $B \to X_s\nu\overline{\nu}$, are dominated by Z exchange. In these models a naive estimate of the ratio of the inclusive rates gives $\mathcal{B}(B \to X_s\nu\overline{\nu})/\mathcal{B}(B \to X_s\ell^+\ell^-) \approx 6$. The factor of six enhancement arises due to a factor of approximately two in the ratio between the neutrino and the charged lepton couplings to the Z, and a factor of three from the sum over the neutrino flavors [13]. A more precise calculation can increase the above ratio up to 7.

Only a subset of the models providing extensions to the SM will be discussed herein. Such models naturally fall into two categories: constrained and unconstrained. Constrained models are where existing bounds from other FCNC processes (for the most part $B \to X_s\gamma$) imply that $B \to X_s\nu\overline{\nu}$ cannot exceed the SM prediction by a factor larger than 2. In unconstrained models however the couplings responsible for enhancing $B \to X_s\nu\overline{\nu}$ are to a large extent independent of those constrained by other existing experimental bounds. Therefore, even a $B \to X_s\nu\overline{\nu}$ decay rate orders of magnitude above the SM prediction is still consistent with the existing constraints and new limits may represent stringent bounds on NP processes. Three models will be briefly mentioned: minimal supersymmetric model (MSSM), multi-Higgs doublet model (MHDM) and supersymmetry(SUSY) with broken R-parity. In our classification above the first two of these are constrained whereas the third is unconstrained.

The MSSM (for review see [14]) is known to produce large effects on the radiative decay $B \to X_s\gamma$, as well as on $B \to X_s\ell^+\ell^-$ (see [15, 16]). The effect on $B \to X_s\nu\overline{\nu}$ have been studied in [16, 17]. It was found that the contributions to the rate can be non-negligible only for $\tan\beta$ close to unity, while for increasing values of $\tan\beta$ the prediction rapidly converges to the SM value, regardless of other SUSY parameters. It is conceivable that a specific choice of SUSY parameters, with a "fine-tuned" MSSM could produce a considerably enhanced $\mathcal{B}(B \to X_s\nu\overline{\nu})$ however such a choice is regarded as unnatural [13]. Feynman diagrams that could contribute to the branching ratio of $B \to X_s\nu\overline{\nu}$ through this model are given in figure 3.

MHDM (for review and notation see [15, 18]) are severely constrained by $B \to X_s\gamma$, $Z \to b\overline{b}$, $B \to X_c\tau\overline{\nu}_\tau$ and lepton universality in tau decays. The same is true for the more familiar two Higgs doublet model (2HDM), which represent a subclass of the general MHDM with natural flavor conservation. In a general MHDM, the single parameter $\tan\beta$ of the 2HDM is replaced by three complex couplings constants. The new Z penguin diagrams present in these models are related to new photonic penguins, and thus are severely constrained by $B \to X_s\gamma$ and cannot contribute significantly to $B \to X_s\nu\overline{\nu}$. The implication of this, along with the small contribution to the box diagram constrained from the previously mentioned, accurately measured reactions from LEP, is that the enhancement of $B \to X_s\nu\overline{\nu}$ has to be very small in this model.

In SUSY models it is usually assumed that R-parity is a good symmetry. However, this is not
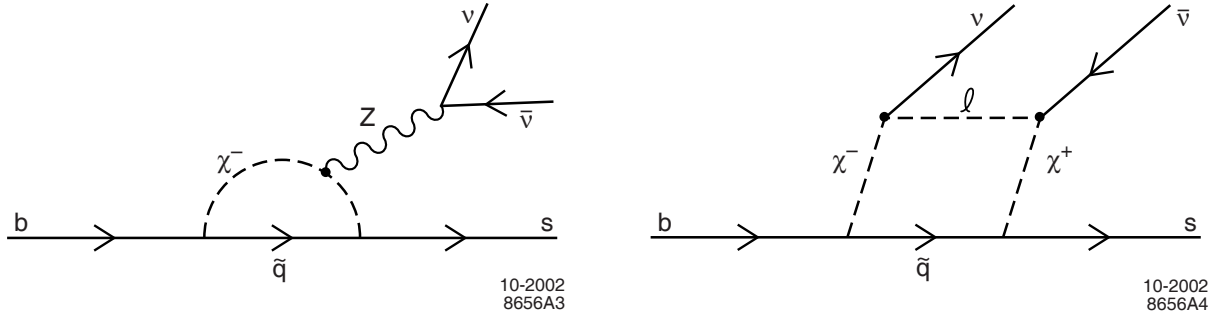
Figure 3: MSSM Feynman diagrams for $B \to X_s \nu \overline{\nu}$

necessarily the case, and one can construct SUSY models with broken R-parity. It seems natural to focus on the MSSM with broken R-parity [19]. Some of the extra couplings allowed in this model can give rise to a large enhancement of the $B \to X_q \nu \overline{\nu}$ decay rate. The main phenomenological changes to the MSSM are that the lightest supersymmetric particle (LSP) is no longer stable and supersymmetric particles can be produced singly at colliders. This can have profound consequences experimentally. One could presuppose a heavy neutral particle, which is considered to be the lightest neutralino, χ_1^0, and also assumed to be the LSP. The neutralino χ_1^0 decays via $O_{\not R_p}$, where $O_{\not R_p}$ is the dominant R-parity violating operator. As far as $B \to X_q \nu \overline{\nu}$ is concerned the χ_1^0 could produce an enhanced rate by replacing the Z^0 in the penguin diagram in figure 1.

For further information on NP effects in $B \to K^{(*)} \nu \overline{\nu}$ see [6, 13, 17, 20–24]

2 $B^+ \to K^+\nu\overline{\nu}$ analysis

2.1 The dataset

The data used in this analysis were collected with the *BABAR* detector, which is described elsewhere [1], at the PEP-II storage ring. The integrated luminosity used in this analysis is $50.7\,\mathrm{fb}^{-1}$ recorded at the $\Upsilon(4S)$ resonance, corresponding to 56.3×10^6 $B\overline{B}$ events, and $6.4\,\mathrm{fb}^{-1}$ taken at energies just below $B\overline{B}$ threshold. This provides a factor of approximately 5 times larger dataset than has previously been used to study this channel at the $\Upsilon(4S)$ resonance [7]. This resonance decays into $B\overline{B}$ pairs with an energy release small enough to preclude the production of any additional particles (other than perhaps soft photons). Simulated data samples for the processes $e^+e^- \to B\overline{B}$, $e^+e^- \to q\overline{q}$ ($q = u$, d, s or c) and $e^+e^- \to \tau^+\tau^-$, in quantities comparable to the data, are used to study backgrounds. A sample of $280\,000$ simulated B^+B^- events with $B^+ \to K^+\nu\overline{\nu}$ and the other B decaying generically have also been analyzed. The simulation of $B^+ \to K^+\nu\overline{\nu}$ decay is based on the form factor model in Ref. [6].

2.2 Analysis method and tagging techniques

The presence of two neutrinos in the final state makes the search for $B^+ \to K^+\nu\overline{\nu}$ difficult, since no kinematic constraints can be applied to the signal B. The strategy adopted in this analysis is to reconstruct exclusively the decay of one of the B mesons in the event, referred to as the "tag" B, and to compare the remaining particle(s) in the event with the signature expected for the decay $B^+ \to K^+\nu\overline{\nu}$.

In order to search the greatest possible subset of events for a decay consistent with that expected from $B^+ \to K^+\nu\overline{\nu}$, the number of tagged events needs to be as large as possible. Therefore a tagging technique with a high reconstruction efficiency is desired. Ideally the exclusive reconstruction of all decay products from the tag B would be preferred. However in practice this is not always possible and instead a sufficient subset of the particles involved in the tag B decay are reconstructed, tagging the B flavor and leaving the remainder of the event to search for a possible signal. Two tagging techniques presented themselves as feasible: a fully hadronic tag and a semi-leptonic tag. The two methods differ in the modes used to tag and remove the daughters of the B meson decay. The semi-leptonic technique reconstructs $B \to Y_c\ell\nu_\ell$ while the fully hadronic technique reconstructs $B \to Y_cQ$, where Y_c denotes either a charged or neutral D meson and Q can be number of K^+, π^+ and/or π^0 mesons. The method is to use the Y_c meson as a "seed" and add other particles in the event to this to form a candidate consistent with coming from a B meson. Other combinations are tried in an attempt to form possible composites (D_s^+, K_S^0 etc) from the particles in the Q system. The leptons considered for tagging purposes, ℓ, are either electrons or muons. These two methods are distinct and complimentary in that the initial selection of a high momentum lepton in the semi-leptonic method is explicitly vetoed in the hadronic case. Therefore independent analyses based on the two methods can be readily combined allowing a study of a

Table 3: B decay modes considered as tagging candidates. The branching fraction is given for each of the four possibilities.

Decay Mode	Branching Ratio
$\overline{B}^0 \to D^0 X^+ \ell^- \overline{\nu}$	4.7%
$\overline{B}^0 \to D^+ X^0 \ell^- \overline{\nu}$	5.3%
$B^- \to D^0 X^0 \ell^- \overline{\nu}$	8.9%
$B^- \to D^+ X^- \ell^- \overline{\nu}$	1.1%

larger sample of the available dataset than would be possible with only one such tag reconstruction technique. Feynman diagrams for typical hadronic and semi-leptonic tags are shown in figure 4. The use of hadronic tagging is described in further detail in section 3.

Figure 4: Feynman diagrams for the tagging modes described in the text. A hadronic tag is shown on the left, with a semileptonic tag on the right.

For the purposes of the analysis descibed in section 2, only the semi-leptonic tagging technique will be considered. Table 3 summarizes the possible tagging modes that can be used for both charged and neutral B mesons. In particular the tagging of charged B mesons will be described here as they are used in the search for $B^+ \to K^+ \nu \overline{\nu}$.

The low multiplicity of the signal decay greatly reduces the combinatorial background in the tag reconstruction, allowing the use of decay modes that would not be sufficiently clean in other circumstances. These considerations lead to the use of the semileptonic decay $B^- \to D^0 \ell^- \overline{\nu} \, X$ for the reconstruction of the tag B. The X system is kinematically constrained to be either nothing or a low-momentum pion or photon from a higher mass charm state (i.e. $D^{*+} \to D^0 \pi^+$ or $D^{*0} \to D^0 (\pi^0 \text{ or } \gamma)$). The D^0 is reconstructed in the $K^- \pi^+$, $K^- \pi^+ \pi^- \pi^+$ and $K^- \pi^+ \pi^0$ modes, these are summarized in table 4 with the branching fraction of each mode provided. This method results in roughly 0.5% of B^- decays being reconstructed as tags. Note that particles from the tag B that escape detection will not affect the sensitivity of the analysis to $B^+ \to K^+ \nu \overline{\nu}$ events; the

Table 4: D^0 Decay modes used by this event selection. The D^0 mass is that used in the Monte Carlo. The reconstruction efficiency is the number of reconstructed decays divided by the total number of decays as given from MC truth.

Parent D^0 mass	Decay Mode	Branching Ratio	Reconstruction efficiency (in data)
1.865 GeV/c²	$D^0 \to K^-\pi^+$	$(3.80 \pm 0.09)\%$	3.3×10^{-3}
	$D^0 \to K^-\pi^+\pi^+\pi^-$	$(7.46 \pm 0.31)\%$	1.0×10^{-3}
	$D^0 \to K^-\pi^+\pi^0$	$(13.10 \pm 0.90)\%$	2.1×10^{-3}

reconstructed $D\ell$ needs to be a correct, but not complete, subset of the particles produced in the tag B decay. The feed-down from higher-mass charm states often results in good tags in this sense, and thus in an enhanced tagging efficiency. This tagging efficiency can be compared to that of a fully exclusive hadronic tag mode which records approximately 0.15% of B^- decays as tags.

The event selection proceeds as follows. Selected hadronic events are required to have an identified electron or muon with a momentum above 1.3 GeV/c in the $\Upsilon(4S)$ rest frame. The electron identification is based on quantities from the electromagnetic calorimeter (EMC), the ring-imaging Cherenkov detector (DIRC) and the gas (DCH) and silicon (SVT) tracking devices. The muon identification uses information from the instrumented flux return (IFR) in addition to the devices listed previously. Loose consistency requirements are placed on the charged particle
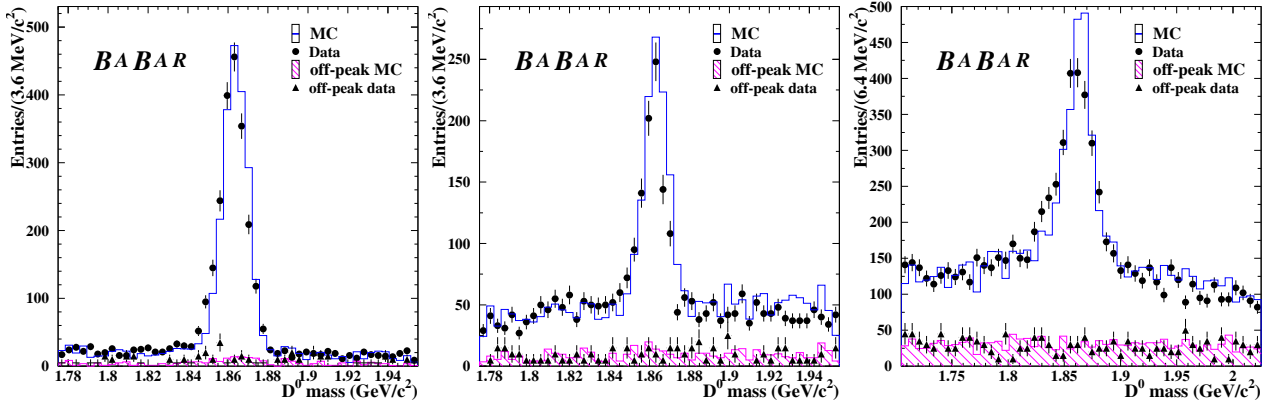

Figure 5: The candidate D^0 invariant mass distributions are shown, from left to right, in the $K^-\pi^+$, $K^-\pi^+\pi^-\pi^+$ and $K^-\pi^+\pi^0$ modes for data (points) and simulation (histogram), for events with no more than three charged tracks and less than 1 GeV of neutral energy not assigned to the tag B candidate. Events are required to have no more than three charged tracks not associated with the tag B in order to mimic the low multiplicity of the signal while maintaining adequate statistics in the plots. The off-resonance distributions have been scaled to the on-peak data luminosity.

vertices for the D^0 and $D^0\ell^-$ candidates. The following kinematic requirements are imposed:

$p^*_{D^0} > 0.5\,\mathrm{GeV}/c$, $m_{D^0\ell^-} > 3\,\mathrm{GeV}/c^2$ and $-2.5 < \cos\theta_{B,D\ell} < 1.1$, where $p^*_{D^0}$ is the momentum of the D^0 in the $\Upsilon(4S)$ frame, $m_{D^0\ell^-}$ is the mass of the $D^0\ell^-$ combination and

$$\cos\theta_{B,D\ell} = \frac{2\,E_B E_{D\ell} - m_B^2 - m_{D\ell}^2}{2\,|\vec{p}_B||\vec{p}_{D\ell}|} \quad . \tag{9}$$

Here E_B and $|\vec{p}_B|$ are respectively the energy of and magnitude of the momentum of the B meson in the $\Upsilon(4S)$ frame. E_B is one half of the center-of-mass energy of the e^+e^- initial state, and $|\vec{p}_B|$ is $\sqrt{(E_B^2 - m_B^2)}$. The upper limit on $\cos\theta_{B,D\ell}$ is 1.1 to account for resolution on the measurement (the signal cannot exceed 1). The lower limit is relaxed to increase efficiency for the feed-down from decays of the type $B^- \to D^{*0}\ell^-\overline{\nu}$ and $B^- \to D^{**0}\ell^-\overline{\nu}$. The requirement on $\cos\theta_{B,D\ell}$ is the most important for restricting the kinematics of the $D^0\ell^-$ to be consistent with coming from a semileptonic B decay. In cases where more than one $D^0\ell^-$ candidate is reconstructed, the one with the smallest value of $|\cos\theta_{B,D\ell}|$ is used. The reconstructed D^0 invariant mass distributions are shown in Fig. 5.

Once the tag B is selected, additional requirements are placed on the remaining particles in the event. There must be exactly one charged track in the event that is not part of the tag B, its charge must be opposite to that of the tag lepton, and it must satisfy the particle identification criteria for charged kaons, which are based on information from the DIRC and tracking system. The momentum spectrum, in the $\Upsilon(4S)$ rest frame, for the kaon from $B^+ \to K^+\nu\overline{\nu}$ decays peaks near the upper kinematic limit while the spectrum for background peaks at low momentum; the signal kaon candidate is thus required to satisfy $p^*_K > 1.5\,\mathrm{GeV}/c$ (see Fig. 6). The angle $\theta^*_{K,\ell}$ between the charged lepton and the signal kaon is isotropically distributed in signal events, since these particles originate from different B mesons, while the background from $e^+e^- \to q\overline{q}$ and $e^+e^- \to \tau^+\tau^-$ peaks forward and backward in this angle; we require $-0.9 < \cos\theta^*_{K,\ell} < 0.8$. In addition to the above requirements on charged tracks, we use information from the EMC and IFR to limit additional neutral particles in the event. The $B^+ \to K^+\nu\overline{\nu}$ signal leaves very little neutral energy in the detector and does not contain any neutral hadrons. We therefore require that the number of IFR clusters consistent with neutral hadrons (N_{IFR}) be zero, and that the energy deposited in the EMC, once the daughters from the $D\ell$ have been removed, (referred to as E_{left} or remaining neutral energy) satisfies $E_{\mathrm{left}} < 0.5\,\mathrm{GeV}$ (see Fig. 6).

The yields in the signal and sideband regions at each stage in the application of the selection criteria are given in Table 5 for the on-peak data and background Monte Carlo, along with the efficiency for the signal Monte Carlo. The distribution of events in the search plane defined by the variables[4] E_{left} and $(m_D - m_D^{\mathrm{fit}})/\sigma_D^{\mathrm{fit}}$ is shown in Fig. 7. The signal box is defined by the requirements $E_{\mathrm{left}} < 0.5\,\mathrm{GeV}$ and $|m_D - m_D^{\mathrm{fit}}| < 3\sigma_D^{\mathrm{fit}}$. The expected background from the Monte Carlo is 2.2 events.

In order to minimize experimental bias, the signal region was hidden until the selection criteria were finalized. In order to evaluate how well the simulation describes the data, we define auxiliary

---

[4]The quantities m_D^{fit} and σ_D^{fit} are the mean and sigma from Gaussian fits to the D^0 invariant mass spectrum. Separate values are calculated for each D^0 decay mode in data and simulation.
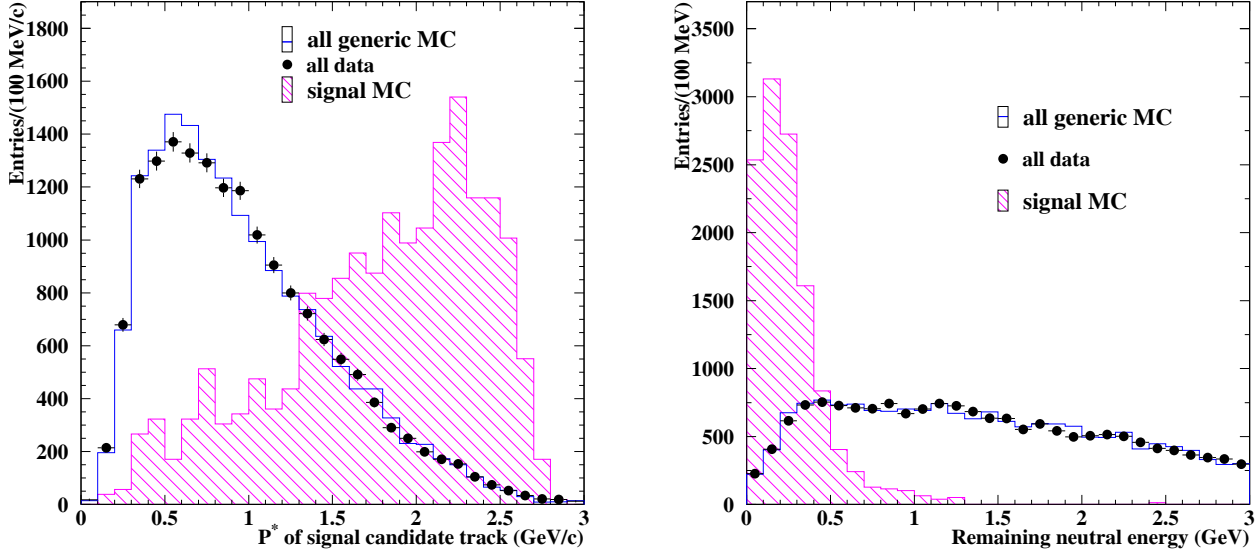
Figure 6: The distributions of p_K^* and E_{left} for simulated signal and background events. Events with no more than three charged tracks and less than $1\,\text{GeV}$ of neutral energy not assigned to the tag B candidate are used for the plot on the left whereas the neutral energy requirement is relaxed to be less than $3\,\text{GeV}$ for the plot on the right. The generic MC distribution has been scaled to the on-peak data luminosity with an arbitrary scale factor applied to the signal MC distribution.

Table 5: The number of events passing the selection criteria for on-peak data, on-peak Monte Carlo contributions, off-peak data, off-peak Monte Carlo contributions and $B^+ \to K^+\nu\overline{\nu}$ signal Monte Carlo efficiency. The number of events in the Monte Carlo sample are scaled to the equivalent luminosity in data. The values include the correction factors for tag efficiency, E_{left} and N_{IFR} referred to in the text.

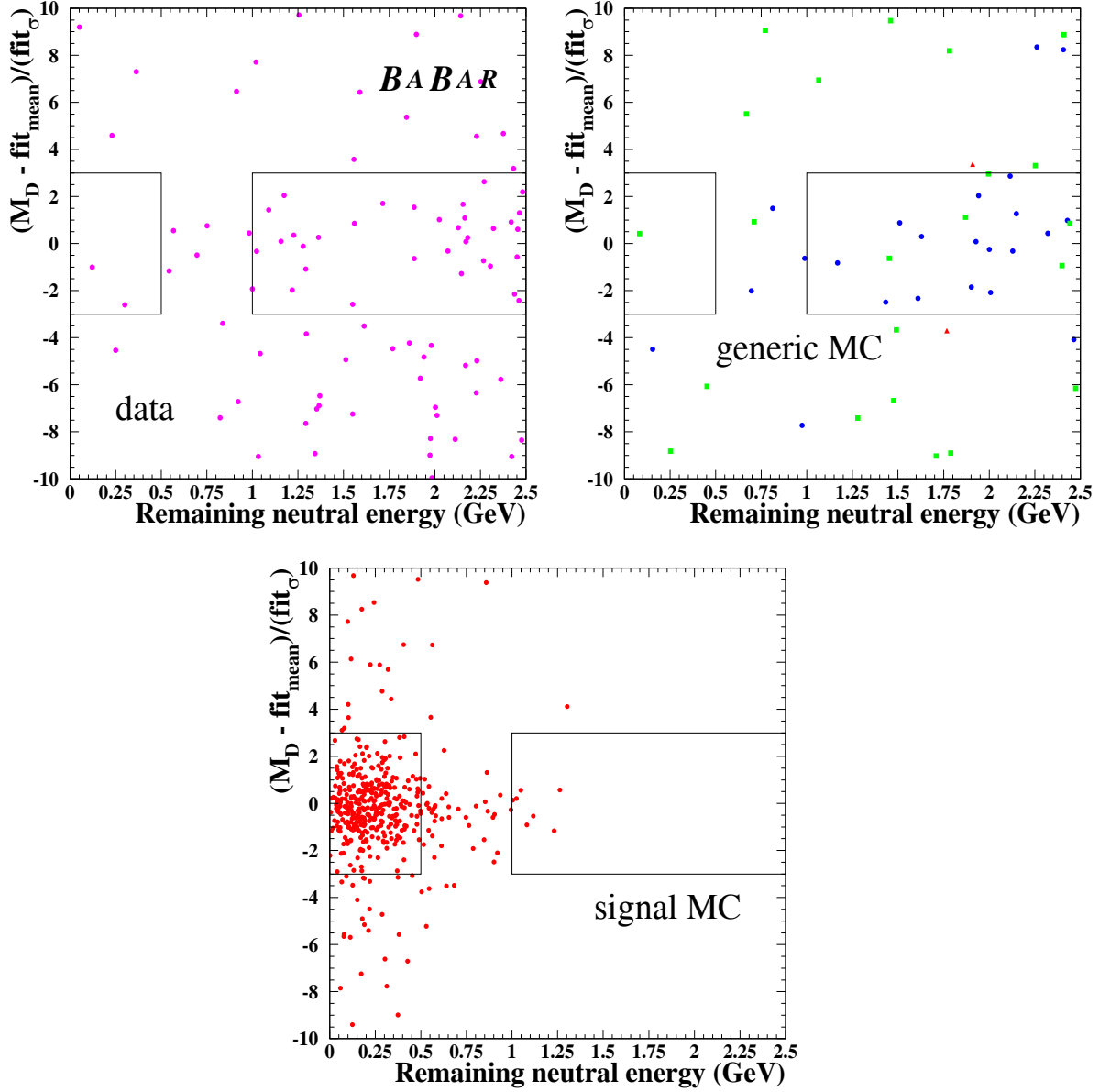|	On-peak ($50.7\,\text{fb}^{-1}$)		Off-peak ($6.4\,\text{fb}^{-1}$)		signal MC
Requirement	data yield	MC yield	data yield	MC yield	effic $\cdot 10^4$
Tag, no extra tracks	8998	8525.7	415	389.9	34.3
Kaon identification	717	707.4	49	46.8	24.3
$\cos\theta_{K,\ell}^*$	485	486.2	32	25.0	20.9
p_K^*	101	89.4	7	5.1	14.2
N_{IFR}	79	72.5	6	4.4	12.0
E_{left} sideband	34	27.4	3	1.4	0.2
D^0 mass sideband	4	7.1	1	0.8	2.0
Signal box	2	2.2	0	0.3	10.3

Figure 7: The distribution of events in the $(m_D - m_D^{\text{fit}})/\sigma_D^{\text{fit}}$ versus E_{left} plane for on-peak data, generic $B\overline{B}$ and continuum Monte Carlo and signal Monte Carlo. In the generic Monte Carlo plot the circles show the contribution from $B\overline{B}$ events, the squares show the contribution from $c\overline{c}$ and the triangles show the contribution from $u\overline{u}/d\overline{d}/s\overline{s}$. The MC has not been scaled to the data luminosity.

samples. Two sideband regions are studied: the D^0 mass sideband, defined by the conditions $|m_D - m_D^{\text{fit}}| > 3\sigma_D^{\text{fit}}$ and $E_{\text{left}} < 0.5\,\text{GeV}$, and a sideband where the additional neutral energy is required to be in the range $1.0 < E_{\text{left}} < 2.5\,\text{GeV}$. The D^0 mass sideband contains incorrectly reconstructed B decays and continuum events whereas the E_{left} sideband is sensitive to correctly reconstructed B tags where the other B leaves only a single detected charged track and substantial missing energy, often in the form of neutral hadrons. The event yields in these regions are also listed in Table 5.
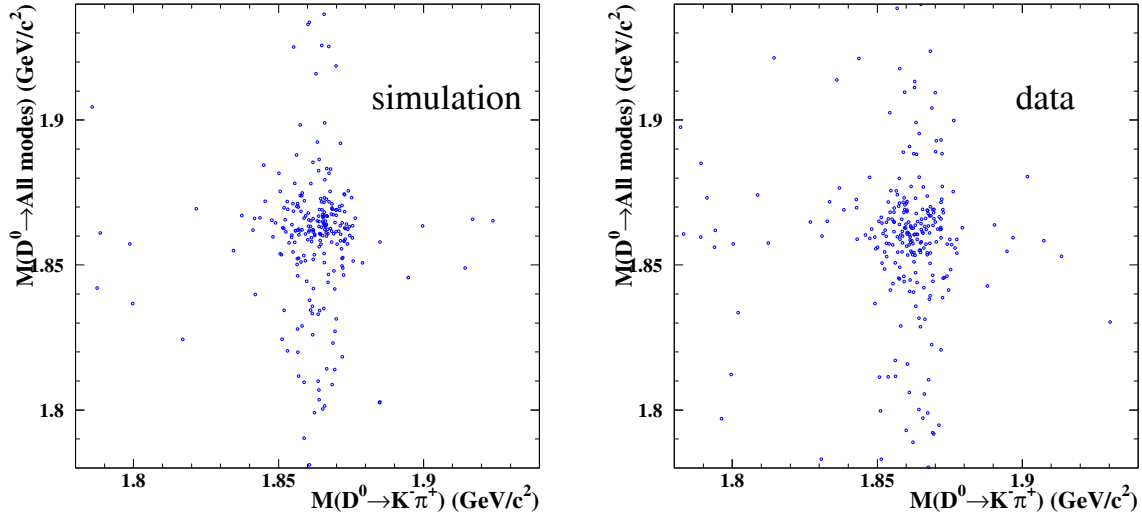

Figure 8: Mass of the $\overline{D}^0$ candidate decaying to all three modes considered versus the $D^0 \to K^-\pi^+$ mass for events in which both B mesons are reconstructed in the $D\ell\,\nu X$ decay mode and no additional charged particles are recorded. The plot on the left (right) shows the results from the simulation (on-peak data).

In addition to the sideband samples, we use "double-tagged" events, in which both B^+ and B^- mesons are reconstructed as $B \to D\ell\nu_\ell$, to quantify the uncertainty in the efficiency of several of our signal criteria. Perhaps due to the high tag efficiency (and hence enhanced tag yield), this is the first time that double-tagged events have been used in *BABAR*. We reconstruct double-tagged events by finding a suitable $D^0\ell^-$ candidate where the D^0 decays to $K^-\pi^+$, and then looking for a second $\overline{D}^0\ell^+$ candidate in any of the accepted $\overline{D}^0$ modes. No particle is assigned to more than one of the $D\ell$ candidates. In addition it is required that the event contain no charged tracks that are not assigned to a $D\ell$ candidate.

The reconstructed invariant masses of the D^0 and $\overline{D}^0$ candidates in double-tagged events that satisfy the above criteria are shown in Fig. 8 for data and for Monte Carlo. After subtracting combinatorial background, the number of double-tagged events satisfying the requirement that
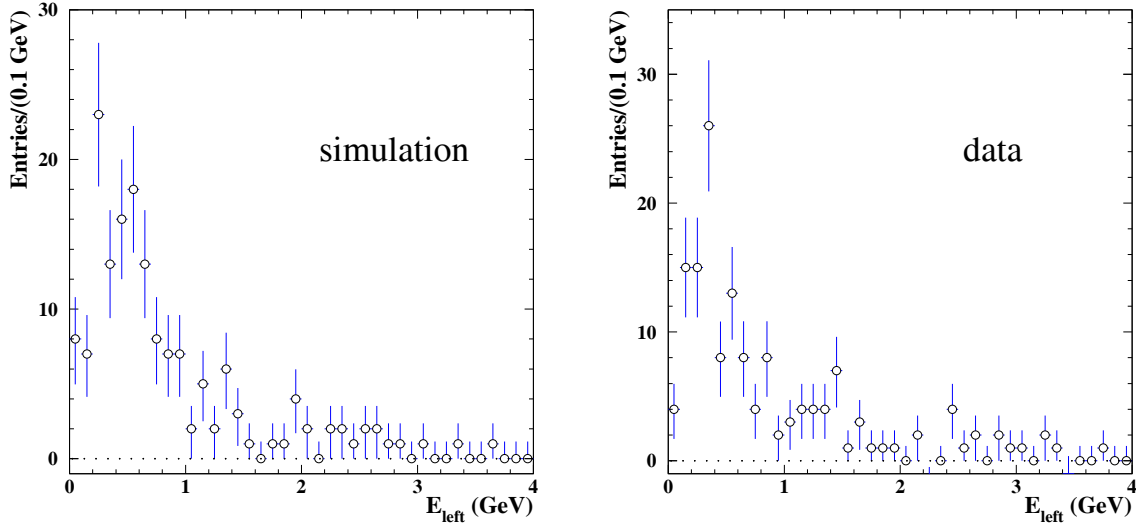
Figure 9: The distribution of E_{left} for "double-tagged" events where both B mesons are reconstructed in the $D\ell\,X$ decay mode and no additional charged particles are recorded. The plots on the left (right) show the distribution from simulation (on-peak data).

$|m_D - m_D^{\text{fit}}| < 3\sigma_D^{\text{fit}}$ for each D candidate is 148 ± 15 in data and 175 ± 16 in the Monte Carlo sample.[5] The number of double-tagged events per fb^{-1} in the data is 0.85 ± 0.11 times the rate in the simulation. This factor is roughly the square of the data/Monte Carlo efficiency ratio for the tag efficiency (including the requirement that there be no additional charged tracks associated with the tag - see the first entry in Table 5). The signal efficiency is therefore corrected by a factor 0.92 ± 0.06, where the uncertainty is taken as a systematic error.

The double-tagged events also allow a study of how well the variables N_{IFR} and E_{left} are simulated. Figure 9 shows the distribution of the E_{left} variable in the double-tagged events; the D^0 mass sidebands have been used to subtract the combinatorial background. The mean values of E_{left} in the data and simulation are $0.91 \pm 0.08\,\text{GeV}$ and $0.84 \pm 0.07\,\text{GeV}$, respectively. The fraction of double-tagged events satisfying the requirement $N_{\text{IFR}} = 0$ is 0.87 ± 0.03 in data and 0.93 ± 0.02 in simulation. These comparisons are used to adjust the simulated signal efficiencies and assign systematic errors.

Systematic uncertainties on the efficiency of selection criteria based on the total number of events with $\Upsilon(4S)$ mesons, tagging efficiency, K selection and momentum, E_{left} and N_{IFR} have all been studied. The total relative uncertainty on the selection efficiency is found to be $\delta\epsilon/\epsilon = 8.7\%$ where the tagging efficiency and E_{left} contribute the largest uncertainties. The systematic uncertainties are summarised in Table 6.

[5] The number of events in the Monte Carlo sample has been scaled to the on-peak data luminosity.

Table 6: A summary of the systematic uncertainties on $\mathcal{B}(B^+ \to K^+ \nu \overline{\nu})$. $\delta\epsilon/\epsilon$ is the relative uncertainty on the overall efficiency.

Quantity	$\delta\epsilon/\epsilon[\%]$
$B\overline{B}$-counting	1.1
Tagging efficiency	6.0
K selection	2.0
$\cos\theta^*_{K,\ell}$	–
E_{left}	4.3
N_{IFR}	3.6
K momentum	1.8

2.3   Physics results

The signal region was unblinded to reveal two events, consistent with the 2.2 events predicted with the simulation. The number of $B^+ \to K^+ \nu \overline{\nu}$ candidates in the data is thus compatible with the background expectation. For the purpose of setting an upper limit, each candidate is assumed to be signal. The Poisson upper limit for 2 events is 5.3. This upper limit must be modified to account for the uncertainty in the efficiency. Using the prescription advocated in [8] increases the upper limit to 5.4 events, from which we find

$$\mathcal{B}(B^+ \to K^+ \nu \overline{\nu}) < 9.4 \times 10^{-5} \quad \text{(preliminary)} \tag{10}$$

at 90% confidence level.

The background at present appears to be mostly combinatorial, based for example on the lack of any D^0 peak in the continuum in Fig. 5. Further refinements may enable this background to be suppressed; the combinatorial component of the background can also be subtracted in the future. The analysis as presented here is included in ref. [9].

Table 7: Expected yields for $B^+ \to K^+\nu\overline{\nu}$ and the associated "tag" B^- reconstruction.

Sample	Efficiency		Theory	Signal Yield			
	Signal	Reco	prediction	0.1 ab^{-1}	0.5 ab^{-1}	2 ab^{-1}	10 ab^{-1}
$B^+ \to K^+\nu\overline{\nu}$	0.3	$(1-1.5)\times 10^{-3}$	4×10^{-6}	0.1	0.7	3	13
	0.2	5×10^{-3}		0.4	2	9	44
	0.2	5×10^{-3}	5×10^{-5}	5	25	113	550
				Background Estimate			
				0.1 ab^{-1}	0.5 ab^{-1}	2 ab^{-1}	10 ab^{-1}
				5	30	140	700

3 Outlook

3.1 Sensitivity

The reconstruction method described in chapter 2 has a number of pertinent features which effect extrapolation to high-luminosity scenarios:

- The overall signal selection efficiency is dominated by the rather low *companion* B^- reconstruction efficiency, rather than the signal B^+ efficiency

- The fact that the signal B^+ has low multiplicity results in a higher purity of the companion B^- reconstruction than would be found for "generic" B^+ decays. This permits the use of B^- reconstruction modes which would be too "dirty" for use in other contexts.

- The companion B^- reconstruction strongly suppresses $B^0\overline{B}^0$ and continuum events compared to B^+B^- events. This dictates that the dominant backgrounds will be due to other B^+ decays faking the signal mode signature provided the companion B^- selection is sufficiently clean. If continuum backgrounds are found to contribute significantly, the selection can be simply be tightened so as to reject it (see section 3.3 for more discussion).

The signal and tag efficiencies and expected yields for $B^+ \to K^+\nu\overline{\nu}$ are given in table 7. The two rows of values correspond to the two different tagging methods for the companion B^- discussed here: semi-exclusive hadronic B reconstruction (top) and semi-leptonic reconstruction (bottom). We speculate the number of expected signal events, given the SM branching ratio for $B^+ \to K^+\nu\overline{\nu}$, in possible future scenarios regarding potential datasets achievable with the current *BABAR* detector and PEP-II machine or some possible upgrade. The current dataset available is close to the 0.1 ab^{-1}, given in the first column of yields in table 7.

In table 7 we also give estimates of the background rates with increasing dataset size and the signal yield (using the semi-leptonic tagging technique only) assuming the $\mathcal{B}(B^+ \to K^+\nu\overline{\nu})$ is anomalously large (5×10^{-5}). We see that for a dataset of 0.1 ab^{-1} the S/B is 1. Assuming that

the detector-related issues regarding K_L^0 simulation for example can be controlled reasonably well by comparing data/MC in control samples and that the backgrounds from decays with unknown branching fractions become further understood one could envision modelling and/or subtracting the majority of the backgrounds present. This would provide the sensitivity for an accurate measurement with a dataset somewhere between 100 and 500 fb^{-1} (i.e. a *BABAR* dataset available within the next 1 to 2 years).

3.2 Background studies

An initial analysis of a subset of the current recorded *BABAR* dataset yielded no evidence for a signal in the $B^+ \rightarrow K^+ \nu \overline{\nu}$ mode. 50.7 fb^{-1} of data taken at the $\Upsilon(4S)$ resonance were used. The current available dataset of *BABAR* has increased throughout the year 2002 to 81.9 fb^{-1} of on-peak data. There has also been a considerable increase in the amount of data recorded below $B\overline{B}$ threshold. This additional data will increase the statistical power of any future search and the off-peak data should enable further studies of contributions to the signal and sidebands regions from non-$B\overline{B}$ processes and combinatorial background. The current upper limit for $\mathcal{B}(B^+ \rightarrow K^+ \nu \overline{\nu})$ is over an order of magnitude away from the SM expectation for this mode (see sections 2.3 and 1.2). Hence it would require a considerable amount of new data, using only the current analysis strategy, in order to reach this level of sensitivity (see table 7). Moreover, since events (which we currently postulate to be background) already populate the signal region with the current dataset one could expect the background to increase as more data is analysed. Indeed the background need not, and probably will not, increase linearly.

As previously noted, relevant backgrounds are predominantly from $B^+ B^-$ events in which the B^- is correctly reconstructed and the B^+ has low observed track and cluster multiplicity in the detector. Such events are caused by a failure to reconstruct observable particles (i.e. particles passing outside of the detector acceptance or falling below kinematic thresholds for tracking or calorimetry), by the presence of neutrinos or unreconstructed neutral hadrons (K_L^0), or a combination of both. Since these backgrounds do not involve cross-feed between the signal and tag B, the background rates should be comparable using either of the tag samples outlined earlier.

Assuming a perfect detector (i.e. using MC truth), topologically irreducible backgrounds to $B^+ \rightarrow K^+ \nu \overline{\nu}$ appear to be at or below the SM rates for this mode, although this does not take into account either the geometrical acceptance or kinematic thresholds for tracking and calorimetry. Applying a more realistic event selection with the present detector configuration yields $B^+ B^-$ backgrounds at the levels of approximately 2×10^{-5}. This, however, is highly uncertain since the branching ratios for B decay modes that mimic the signal when one or more particles are undetected have large uncertainties or are, in some cases, unknown. Therefore it becomes clear that in the absence of additional rejection power signal/background (S/B) is expected to be somewhat less than one for this mode.

In the $B^+ \rightarrow K^+ \nu \overline{\nu}$ mode, more than half of these backgrounds are attributable to B^+ events

containing one or more K_L^0. Note that constraints on the EMC cluster multiplicity and energy already suppress events with a K_L^0 which interacts in the EMC, so the remaining K_L^0 backgrounds are due to IFR-only or "undetectable" K_L^0's. At present, the performance of the IFR is inadequate to permit the use of a meaningful veto on IFR-only K_L^0's. In lieu of this, a veto on any event containing a cluster consistent with coming from a neutral hadron was applied.

The background rate for $B^+ \rightarrow K^+ \nu \overline{\nu}$ is lower than that for other rare decays with missing energy by exploiting three factors: the requirement of a charged kaon suppresses pion backgrounds; the hard momentum spectrum of that signal kaon permits a momentum cut of $p_{CM} > 1.5$ GeV/c; the presence of a charged kaon makes it less likely that there will be K_L^0 (i.e. a second s quark) in the event.

Additional rejection power can likely be obtained beyond the quoted limits by optimization of the selection algorithm, but it is unlikely that the improvement would be dramatic. Because of the relatively low S/B ratio, the $B^+ \rightarrow K^+ \nu \overline{\nu}$ signal would have to be obtained from a small excess of events above a background, most likely using a fit to the candidate signal track momentum spectrum. Since the dominant backgrounds are from B decay modes with low and poorly known branching ratios and containing neutral hadrons which are not well modeled in the present simulation it is likely that these will dominate the determination of $\mathcal{B}(B^+ \rightarrow K^+ \nu \overline{\nu})$. The measurement will be further limited by detector-related systematics.

3.3   Improvement of tagging technique/analysis method

The method used and the extraction of the result presented in chapter 2 could be open to improvement. It is evident from figure 7 that the generic MC distribution contains a considerable background from continuum processes, predominantly from $e^+ e^- \rightarrow c \overline{c}$. The contributions to this background have yet to be studied and suppression of such events is necessary to improve the background rejection. In order to accomplish this, the study of variables not yet used in the selection criteria is required to exploit possible quantities sensitive to $c \overline{c}$ decays. Understanding the processes occurring in such events forms a subset of the overall question of background modeling and subtraction. As more data is analysed more events will be expected to populate the signal and sideband regions in figures 7 as suggested in section 3.2. Therefore understanding the reasons why events are entering these regions will become of greater importance. This will require running more specific MC samples based on prospective background processes to calculate the expected number of events from these decays in the dataset used. Also a detailed study of the level at which particle acceptance becomes a major issue will be necessary. The rate at which loosing particles down the beampipe, hence missing all the sub-detectors, causes an enhancement of signal type decays needs further study.

The total measured EMC energy, E_{left}, of neutral clusters which are not associated with the reconstructed B^- requires further study. For a perfect detector and reconstruction algorithm, this quantity should be zero for signal events however, mis-reconstruction, contributions from hadronic

split-offs, beam backgrounds etc. significantly broaden it for real events. The analysis cut applied in the search for $B^+ \rightarrow K^+ \nu \overline{\nu}$ [9] was $E_{\text{left}} < 500$ MeV. The loss of particles outside of the acceptance causes background events to shift towards low values of E_{left} and hence into the defined signal region.

As suggested in section 3.2 background processes involving neutral hadrons (K^0_L) provide a significant background to the $B^+ \rightarrow K^+ \nu \overline{\nu}$ signal. Improvement in vetoing events containing neutral hadrons either through their neutral calorimeter clusters, IFR clusters or by exploiting some characteristic of their decays (shape variables or angular cuts) would provide a major breakthrough not only for the $B^+ \rightarrow K^+ \nu \overline{\nu}$ analysis but also for further analyses where K^0_L's form a significant fraction of the background (see section 3.5).

3.4   Use of other tagging methods

As was outlined in section 2.2, and mentioned in this chapter, there are other methods of tagging B mesons that were not utilised for the extraction of the limit quoted in section 2.3. Using hadronic B decays to tag one of the B mesons in the event provides a completely distinct and complimentary method to that of tagging via semi-leptonic B decays which was used in the analysis presented here. Since B mesons decay predominantly into hadronic final states involving D or D^* mesons there are many modes in which a suitable tag can be reconstructed via this method. One notes that even if all of the measurable particles associated with the semi-leptonic tag are recorded there will always be some energy lost via the neutrino partner of the lepton. This is not necessarily problematic (and does have some benefits) though as we need to reconstruct a unique but not complete subset of the particle for the semi-leptonic tags. In the hadronic case it is possible to account for all tracks and neutrals from the tag in an exclusive way hence leaving the remainder of the event to search for the signal mode. This allows the use of other kinematic quantities with the two variables usually used to form a plane in which the signal and sidebands can be defined are the beam-energy substituted mass,

$$m_{ES} = \sqrt{E_b^{*2} - (\sum_i \mathbf{p_i^*})^2},$$ (11)

and the invariant energy difference of the B meson candidate

$$\Delta E = \sum_i \sqrt{m_i^2 + \mathbf{p_i^{*2}}} - E_b^*,$$ (12)

where E_b^* is the beam energy in the $e^+ e^-$ rest (CM) frame, $\mathbf{p_i^2}$ is the CM momentum of daughter particle i of the B meson candidate and m_i is the mass hypothesis for particle i. For signal events, m_{ES} peaks at the B meson mass and ΔE peaks near zero, indicating that the candidate system of particles has total energy consistent with the beam energy in the CM frame. Figure 10 [25] shows the m_{ES} distribution for a semi-exclusive hadronic selection. The peak region (using the signal Monte Carlo) is centered at the B meson mass with a tail stretching out to lower masses. We see in

the lower figure the considerable background in this method prior to any selection criteria having been imposed. Note that in reality there would be at minimum a $\cos\theta_{\text{thrust}}$ cut and an additional requirement to correlate the D^0 daughter kaon charge with the charge of the reconstructed B, which brings down the combinatoric background by a factor of two. Neither of the aforementioned cuts have been applied in figure 10.

3.5   Other considerations

The semi-leptonic tagging mode, which has been developed for the search for $B^+ \to K^+ \nu\overline{\nu}$, may find use in the search for other rare modes where missing energy is present. Searches are currently in progress for the decays $B^+ \to \tau^+\nu$, and $B^0 \to \nu\overline{\nu}$ while analyses searching for similar reactions such as $B^+ \to \pi^+\nu\overline{\nu}$, $\overline{B}^0 \to \overline{K}^{*0}\nu\overline{\nu}$ and $B^0 \to \gamma\nu\overline{\nu}$ should be able to utilise the tagging methods described herein.
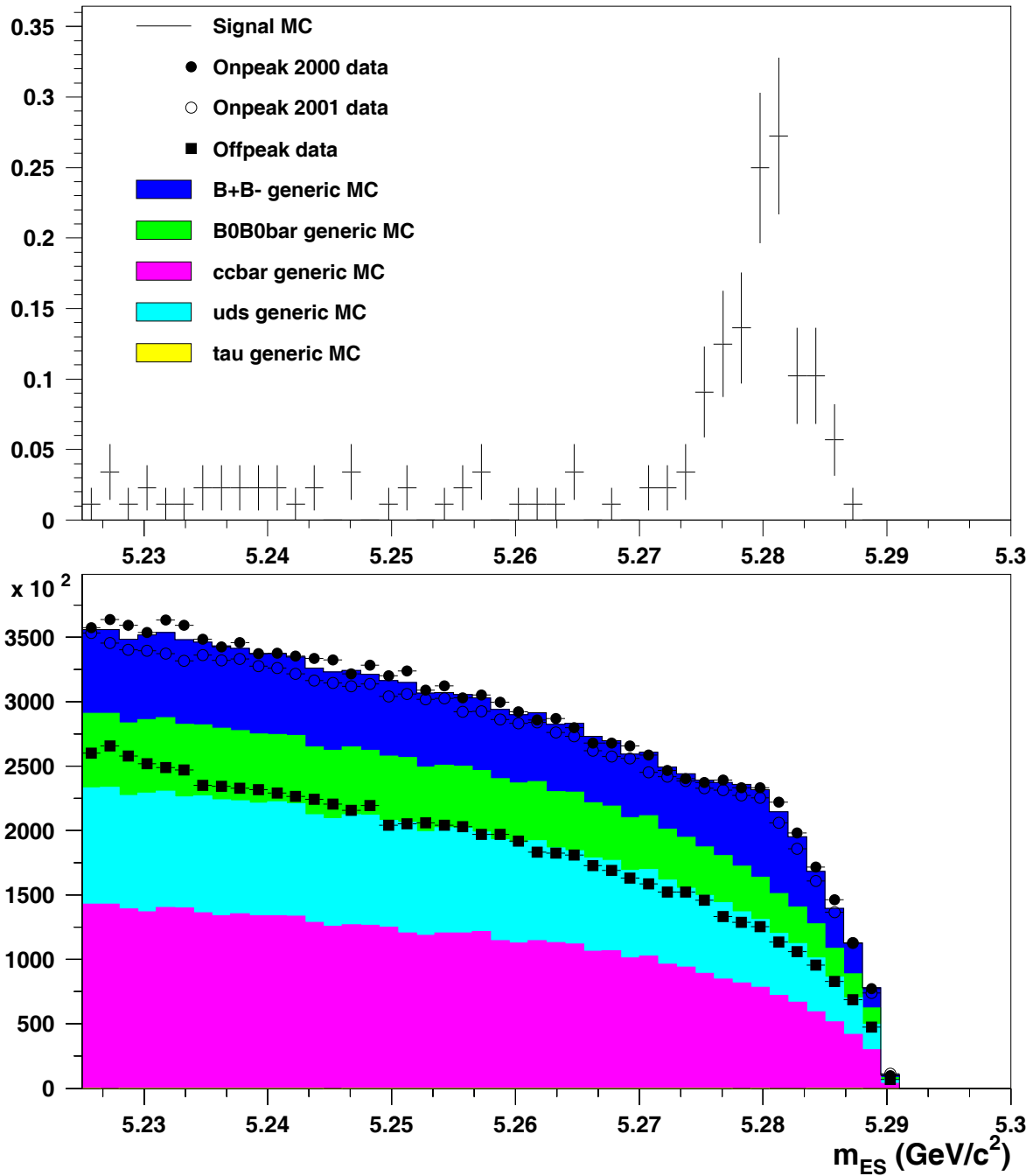
Figure 10: m_{ES} distribution for semi-exclusive hadronic selection.

References

[1] *BABAR* Collaboration, A. Palano *et al.*, Nucl. Instrum. Methods **A479**, 1 (2002).

[2] BELLE Collaboration, K. Abe *et al.*,

[3] CLEO collaboration, R. Ammar *et al.*, Phys. Rev. Lett., **71**, 674, (1993).

[4] CLEO collaboration, M.S. Alam *et al.*, Phys. Rev. Lett., **71**, 2885, (1995).

[5] *BABAR* Collaboration, P. F. Harrison and H. R. Quinn,
    "The *BABAR* Physics Book: Physics at an Asymmetric B Factory," SLAC-R-0504.

[6] G. Buchalla, G. Hiller and G. Isidori, Phys. Rev. D **63**, 014015 (2001).

[7] CLEO Collaboration, T. E. Browder *et al.*, Phys. Rev. Lett. **86**, 2950 (2001).

[8] R. D. Cousins and P. L. Highland, Nucl. Instrum. Methods **A320**, 331 (1992).

[9] *BABAR* Collaboration, A. Palano *et al.*, **hep-ex/0207069**.

[10] *BABAR* Collaboration, A. Palano *et al.*, **hep-ex/0207082**.

[11] BELLE collaboration, K. Abe *et al.*, Phys. Rev. Lett., **88**, 021801, (2002).

[12] CDF collaboration, T. Affolder *et al.*, Phys. Rev. Lett., **83**, 3378, (1999).

[13] Y. Grossman, Z. Ligeti and E. Nardi, Nucl. Phys. **B 465** (1996) 369-398

[14] H.E. Haber and G.L. Kane, Phys. Rep. **117** (1985) 75; H.P. Nilles, Phys. Rep. **110** (1984) 1;
    M.F. Sohnius, Phys. Rep. **128** (1985) 41.

[15] J.F Gunion, H.E. Haber, G.L. Kane and S. Dawson, *The Higgs Hunter's Guide* (Addison-
    Wesley Publishing Co., Reading MA, 1990); and references therein.

[16] S. Bertolini, F. Borzumati, A. Masiero and G. Ridolfi, Nucl. Phys. **B 353** (1991) 591.

[17] C. Bobeth, A.J. Buras, F. Kruger, J. Urban, Nucl.Phys. B. **630** (2002) 87-131.

[18] Y. Grossman, Nucl. Phys. **B 426** (1994) 355.

[19] J. Ellis *et al.*, Phys. Lett. **B 150** (1985) 142.

[20] D. Melikhov, N. Nikitin and S. Simula Phys. Lett. **B 410** (1997) 290-298.

[21] D. Melikhov, N. Nikitin and S. Simula Phys. Lett. **B 442** (1998) 381-389.

[22] T. Barakat J. Phys. G: Nucl. Part. Phys. **24** (1998) 1903-1912.

[23] C. S. Kim, Y. G. Kim, T. Morozumi Phys. Rev. **D 60** (1999) 094007.

[24] T.M. Aliev, A. Ozpineci, M. Savci Phys.Lett.B506:77-84,2001

[25] This figure had been used with the kind permission of Steve Robertson.